Design of GPR for buried object Detection using Ultra Wide Band (UWB) Antenna

P.Upender, P.A.Harsha Vardhini

Abstract— This paper deals the combination of image analysis and EM approach to predict the shape of the cavity detection for satellite remote sensing at 1GHz to 3GHz. The reconstruction of the shape is based on the mean image strength with measured reflectivity at any depth and then with image processing techniques deconvolution. For this purpose, a Vector Network Analyzer has been used along with a Ultra Wide Band antenna, using a stand it is mounted on the sand pit and when operated it moves over it.For a shallow buried object detection system based on image processing and electromagnetic theory, an algorithm has been proposed. The buried utility form is calculated for any depth that is important for the returned echo. Using image analysis and microwave remote sensing techniques to identify the shape of the various shallow buried objects, this approach will be quite helpful in developing an automatic satellite data based information system.

Index Terms: cavity detection, image analysis, Vector Network Analyzer, Ultra Wide Band antenna, remote sensing.

I. INTRODUCTION

Ground penetrating radar (GPR) uses the propagation and dispersion of waves to identify objects and quantitatively perceive changes in the electrical properties of the ground. It can be achieved from the earth's surface, in a borehole or between boreholes, aircraft or satellites.It has the highest resolution of any geophysical system in the underground imagery, exceeding centimeters under the right conditions[1,2].Three distinct techniques have been developed in the field of ground penetrating radar, namely pulse radar, frequency modulated continuous wave radar and stepped frequency continuous wave radar (SFCW) [3].

SFCW – GPR is a form of frequency-domain pulse synthesis that has been commonly used for ground penetration radars. The SFCW radar operates at a high frequency level from a low frequency range. The frequency is modified to cover the required bandwidth in discrete, easily reproducible and stable measures. The phase and amplitude of the received tone is then sampled and the equivalent time-domain sweep reconstructed via an Inverse Fast Fourier Transform [4]. SFCW radar, in principle, measures the same electric and magnetic parameters as conventional carrier free pulsed systems.The sfcw radar gets the range to a target by calculating the coherent target reflections within the specified bandwidth over a number of phase frequencies [5].

The SFCW radar consists of five major sub-systems [6, 7 and 8]:

1. The transceiver: This is responsible for generating the waveforms being transmitted and collecting the waveforms being reflected.
2. The antennas: They pair the transceiver's power into and out of the underground media.
3. The DSP or Digital Signal Processor: The raw spatial frequency data will be transformed into spatial data by this system.
4. The MMI or Man-Machine interface: The MMI includes the DSP configuration and processing code and shows the images on the subsurface.
5. Battery:

The dielectric constant of the target plays an important role in successful detection using SFCW – GPR, the higher the dielectric coefficient of the target, the stronger its reflection is and the better the imaging is. Table 1 shows the various parameters of the SFCW waveform used in this work.

Table 1 SFCW Radar Parameters

S.NO	SFCW Radar parameters	Value
1	Frequency range	1 GHz to 3 GHz
2	Frequency step	10 MHz
3	Number of frequencies	201 points
4	Range Resolution	7.5 cm
5	Unambiguous Range	150 m
6	Investigated Range	1 m
7	Output Power	20 dBm

Visualizing SFCW Ground Penetrating Radar Data

Three types of radar data displays are available: a one-dimensional trace (A- Scan), a two-dimensional cross section (B-scan) and a three dimensional display (C-Scan) [9, 10]. These are briefly described here

(a) A-Scan: After positioning the antenna above the location of interest, A- scan is obtained by stationary calculation, emission and signal collection. The signal obtained is shown as signal strength vs length.

(b) B-Scan or two-dimensional data display signal is derived from the A-Scans ensemble as a horizontal array. The horizontal axis of the two-dimensional picture consists of a cross range (antenna position) and a practically vertical axis (wave propagation path distance from the antenna).

(c) C scan or 3D data presentation signal is obtained fromt he B scans ensemble, calculated by repeated line scans along the plane.

Revised Manuscript Received on October 15, 2019

P.Upender, Asst.Professor, Department of ECE, Vignan Institute of Technology and Science, Deshmukhi, Telangana, India

Dr.P.A.Harsha Vardhini, Professor, Department of ECE, Vignan Institute of Technology and Science, Deshmukhi, Telangana, India

II. METHODOLOGY

2.1 System overview and measurement procedure:

The vector network analyzer used in this experimental work is Rhode and Schwarz VNA (R&S ZVL 3). It is used to generate frequencies in the range of 1 GHz to 3 GHz. The SFCW wave is divided in 201 points by the spacing of 5 cm each. It is capable of giving a maximum power level of 20 dBm. It is operated in SFCW mode and is used for reflection measurement. The VNA is used to measure S11 values which give information about the magnitude and phase of the reflected waves. Figure 1 shows the VNA in use.

Figure 1 Vector Network Analyzer

The coefficient of reflection (S11) is the voltage ratio of the retuned signal voltage level to the signal of the incident. Return loss is used to describe the logarithmic reflection coefficient. The lack of return is used to describe the function of logarithmic reflection. Return loss is the number of decibels below the incident signal that is mirrored. The antenna used is the double ridged waveguide horn antenna Rhode and Schwarz-HF 906, a compact broadband transmitting and receiving antenna for the 1GHz to 18 GHz frequency range.

The RF connector is N female and the nominal impedance is 50Ω. The gain of the antenna is 8 to 10 db from 1 to 3 GHz. Figure 2 shows the antenna and the sand pit used in the experimental work.

Figure 2 Rhode and Schwarz Antenna and Sand Pit

2.1 Data Collection

The sand pit as shown in Figure 2 was divided into a grid of 21 by 21 points spaced at a distance of 5 cm from each other. During the course of the experiments water was continuously added to the sand after each set of experiment in order to study the effect of moisture on the imaging and detection. The antenna is located at a height of 10 cm above the sand surface and the objects are buried in the sand at different depths. The antenna is mounted on a movable platform where it can slide in two transverse directions above ground. The transmitted signal is stepped up from 1 GHz to 3 GHz in 201 steps with each frequency step being 10 MHz. The values of S11 depend on the dielectric constant of the medium. Wherever there is a change in the dielectric constant, reflections occur. Further this data is transferred to MATLAB and signal processing algorithms are applied to locate any cavity or metal in the sand pit. Figure 3 shows the three targets buried in the sand pit.

Figure 3 Image of the cavity, metal sheet and water bottle buried in sand

Table 2 Target Parameters

Target type	Target size	Dielectric Constant
Air cavity	30 cm by 18 cm by 18cm	1
Metal sheet	25 cm by 25 cm	∞
Water Bottle	30cm , diameter 10 cm	80

Following is the flowchart that shows the data collection procedure

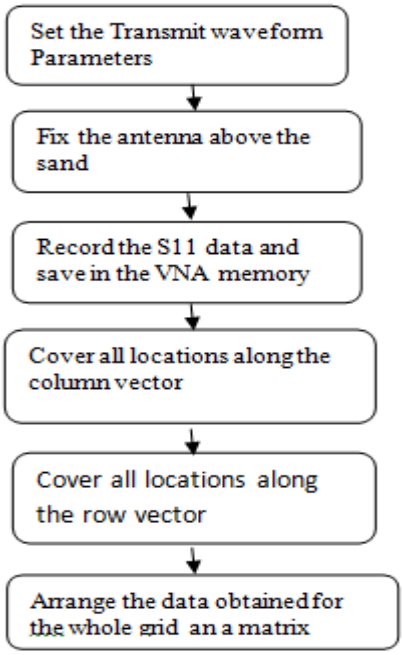

The procedure is repeated by changing depths of buried objects from 5cm to 15cm, also after each set is completed, water is added in the sand pit to increase the dielectric constant of the sand. Moisture content is gradually increased from 5.65% to 15.98%. Table 2 gives description of the experiments conducted in the sand pit setup as described above. The dielectric constant of the wet sand can be computed as

$$\varepsilon = (a_0 + a_1 S + a_2 C) + (b_0 + b_1 S + b_2 C) m_v + (c_0 + c_1 S + c_2 C) m_v^2 \quad \text{.....(1)}$$

a_0 =2.862, a_1 =-0.012, a_2 =0.001, b_0 =3.803, b_1 =0.462, b_2 =-0.341, c_0 =119.0036, c_1 =-0.5, c_2 = 0.63

m_v is the moisture content in the soil.

III. IMPLEMENTATION AND RESULTS

The method for plotting A- scan, B-scan and C- scan is discussed. Received data is in frequency domain which is converted to time domain using IFFT. The time domain signal is plotted as signal strength verses time delay. In the plot obtained peaks are looked for where reflections occur and location of the discontinuity is obtained. The antenna and soil reflections are further recorded and ignored by background subtraction methods. The Figures 4-9 shows the A-Scans, B-scan and C- scan results in the absence and presence of the target and after background subtraction is done.

A-Scan imaging:

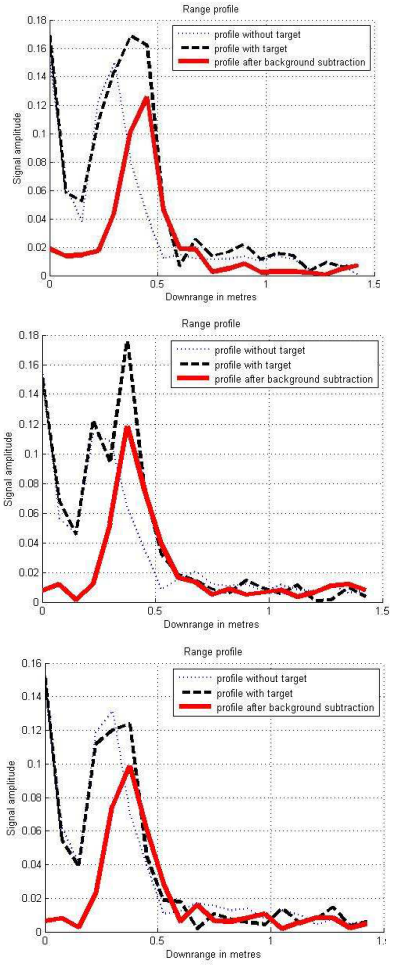

Figure 4 A-scan of metal buried at 5cm, 10cm and 15 cm below surface

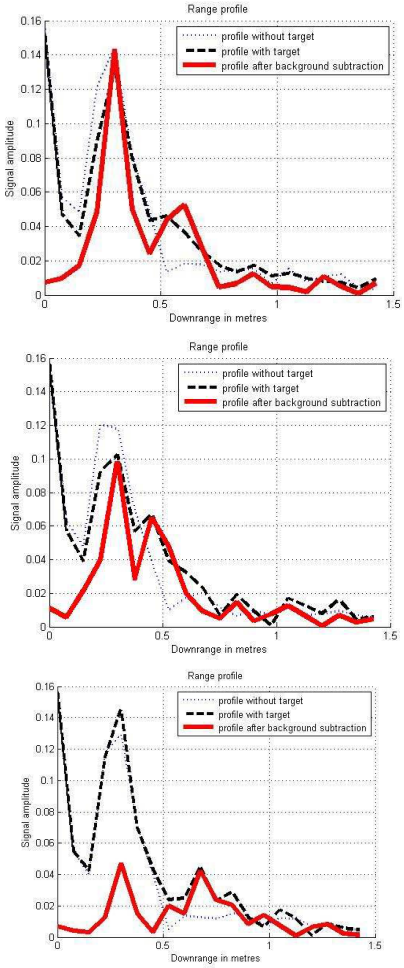

Figure 5 A-scan of cavity buried at 5cm, 10cm and 15cm below surface

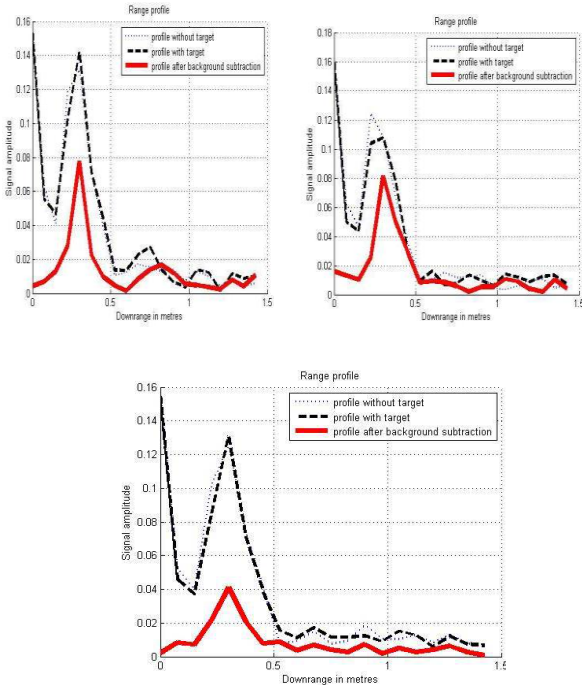

Figure 6: A-scan of cavity buried at 5cm, 10cm and 15cm below surface

It is observed that the reflection amplitudes are weaker than in the case of air cavity. Also at the depth of 15 cm the difference between the peak due to the presence of the water bottle and that due to the noise elements is not significant and hence A – Scan detection fails here, requiring B and C Scans for proper imaging. Figure 6 shows the graphical representation as of why the imaging and detection of the water bottle is difficult as compared to the cavity.

B Scan Imaging:

For B Scan imaging A-Scans are clubbed along a dimension of the sand pit resulting in the formation of a 2D image. This results in a more complete view of the subsurface under study. The image is formed with the Scanning direction horizontally, and the distance vertically. In the beginning the raw B – Scan image of the subsurface is plotted. Figure 7 shows the B Scan image of a cavity buried in the subsurface at a depth of 10 cm below surface and 20 cm below the antenna.

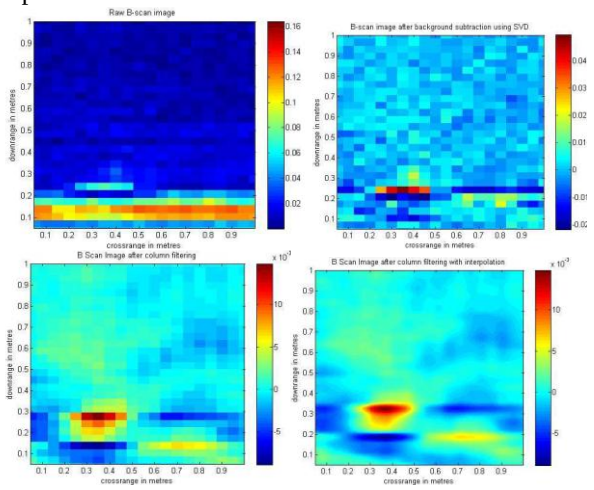

Figure 7 Scan image of cavity at depth of 20 cm below antenna after column filtering

After application of column filtering and interpolation, it is observed that there are no steep transitions in the image pixels. Also column filtering is done by choosing the size of the filtering window as 4 X 4 pixels. The reason for this is that the swath of the antenna illuminates this much area at the position it is placed above the sand grid. For interpolation, 10 values are found out in the grid spacing of 5 by 5 cm. After these two algorithms are applied, the cavities presence is very clear.

Application of Back – Projection Data on Raw B Scan Image

The method of processing the experimental B Scan data obtained is to use the back projection algorithm instead of clutter removal – singular value decomposition.

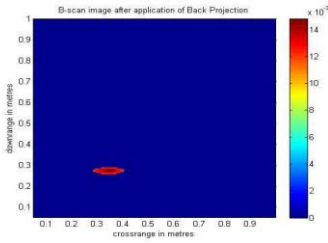

Figure 8: B Scan image of cavity buried 20 cm below antenna after back-projection

The C-Scan is taken from the B-Scans ensemble. The C-Scan approach adds another dimension to B Scan's measured data. It acquires a three-dimensional data set in both cross-range directions with the Scanning coordinates and the down-range time / depth coordinate. For C-Scan, the two-dimensional image is plotted by taking a fixed depth plane chosen by observing the profile of the array.

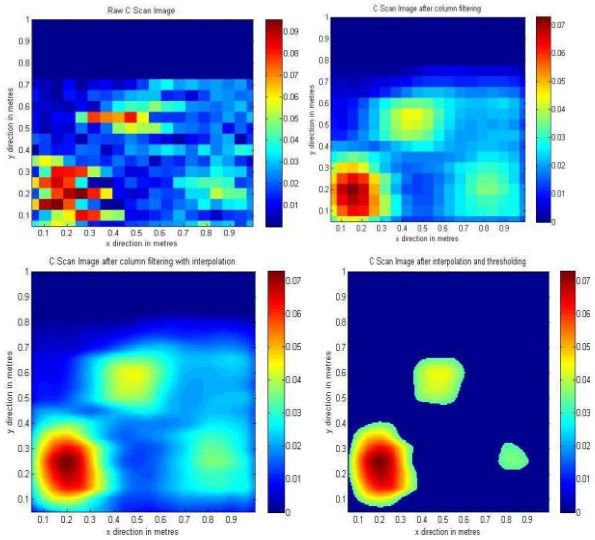

Figure 9: C scan images (i) Raw image after applying (ii) column filtering (iii) Interpolation (iv) Thresholding

In the above, first image is the Raw C Scan image at burial depth 5 cm. Second image is the C Scan image after column filtering at burial depth 5 cm. Third image is the C Scan image after interpolation at burial depth 5 cm. Fourth image is the C Scan image after thresholding at burial depth 5 cm. C Scan image after thresholding at burial depth 5 cm.

This result in background subtraction and only the buried targets of interest are visible in the image. The information about the targets is now more prominent after the application of thresholding. The dark core in the left hand side target is metal, while the other two targets having lighter texture are cavity and water. It is also observed that if the threshold function is increased the detection of the cavity and water bottle would not be possible. Hence a balanced threshold is required. A large threshold results in the ignorance in the detection of an object. A smaller threshold would result in inclusion of unnecessary noise in the C Scan image.

IV. CONCLUSION

The imaging and identification of the various targets buried at depths from 5 cm to 15 cm, and increasing moisture content was successfully done. The objects successfully detected, imaged and identified were a metal sheet, air cavity and a water bottle. The imaging resulted in detection through identification using processes such as A Scan, B Scan, C Scan, clutter removal using singular value decomposition, column filtering, interpolation and thresholding. It was observed that the detection of metal was the easiest, followed by the cavity and then the water bottle. The imaging and identification was easier for those targets whose dielectric

coefficient is much stronger than that of the sand medium, because the reflections are much stronger in these cases. The resulting plots depict that at increasing depths the reflections become weaker, the strongest being at 5 cm and weakest at 15 cm. The experimental results showed that the imaging and detection of buried objects is becomes easier with increasing moisture levels for lesser depths as compared to the resolution , while for objects buried deeper show the inverse effect and hence in these cases the detection and imaging becomes difficult with increasing moisture level.

REFERENCES

1. A. Suksmono, A. Pramudita, E. Bharata, A. A. Lestari, and N. Rachmana, " A Novel Design of the Stepped Frequency Continous Wave Radars Based on Non – Uniform Frequency Sampling Scheme" , Proceedings of the International Conference on Electrical Engineering and Informatics , pp – 270-273, June 17-19,2007
2. C. Gilmore, D. Collins, S. Peters "Design, implementation and testing of a prototype 1.1-2.1 GHz SFCW GPR for use in landmine detection" , Canadian Conference on Electrical and Computer Engineering, pp 291-296, Vol. 1,2002.
3. G.A. Ybarra; G.L. Bilbro; S.M. Wu; S.H. Ardalan; C.P. Hearn; R.T. Neece, "High resolution target range estimation using frequency-stepped CW radar", IEEE MTT-S International Microwave Symposium Digest, pp 249-252, 1993.
4. G. Alberti, L. Ciofaniello, M. D. Noce, S. Esposito, G. Galiero, R. Persico, M. Sacchettino and S. Vetrella, "A stepped frequency GPR system for underground prospecting", Annals of Geophysics, Vol. 45, No. 2, April 2002
5. A. Langman, S. P. Dimaio, B. E. Burns and M. R. Inggs, "Development of a Low Cost SFCW Ground Penetrating Radar" , International Geoscience and Remote Sensing Symposium, pp 2020-2022, Vol. 4 1996.
6. S. Hamran and K. Langley, "A 5.3 GHz Step-Frequency GPR for Glacier Surface Characterisation", Tenth International Conference on Ground Penetrating Radar,pp 1-4, 21-24 June, 2008, Delft, The Netherlands
7. A. Langman, M.R. Inggs, "A 1-2 GHz SFCW radar for landmine detection", Proceedings of the 1998 South African Symposium on Communications and Signal Processing , pp 453-454 , 1998
8. C. Rennie,, B. Arendse, M.R. Inggs, A. Langman,, " Practical measurements of land mine simulants using a SFCW radar, a pulse induction metal detector and an infrared camera" , Second International Conference on the Detection of Abandoned Land Mines,pp 182-186, 1998
9. P. K. Verma, A. N. Gaikwad, D. Singh, and M. J. Nigam, " Analysis of clutter reduction techniques for through wall imaging in UWB range" , Progress In Electromagnetics Research B, Vol. 17, pp 29-48, 2009.
10. R. Chandra, A. N. Gaikwad, Dharmendra Singh and M J Nigam, " An approach to remove the clutter and detect the target for ultra – wideband through wall imaging", Journal of Geophysics and Engineering, pp 412-419, Vol. 5, 2008.

AUTHORS PROFILE

P.Upender received B.Tech degree from JNTU, Hyderabad, M.Tech degree in RF & Microwave from IIT ROORKEE and pursuing Ph.D. He is currently an Assistant Professor in the department of Electronics and Communication Engineering at Vignan institute of technology and sciences, deshumuki. His research interests are microwave engineering, Antennas, Radar Engineering, RF communication.

Dr. P.A.Harsha Vardhini, professor in the Department of Electronics and Communication, Vignan Institute of Technology and Science, Deshmukhi has 18 years of teaching experience. She pursued her Ph.D in VLSI Design from the department of ECE, JNTUH. Her research interests include Low Power Mixed Signal VLSI Design, FPGA architectures, IoT Embedded Applications & Wireless Communication. She is an IEEE & WIE member and life member of IEI, ISOI, IAENG, IAOE. She has more than 90 publications in various journals and conferences at national and International level including SCI, SCOPUS, IEEE, Springer, Elsevier and UGC.